ON A SCHRÖDINGER–LANDAU–LIFSHITZ SYSTEM: VARIATIONAL STRUCTURE AND NUMERICAL METHODS*

JINGRUN CHEN†, JIAN-GUO LIU‡, AND ZHENNAN ZHOU§

Abstract. From a variational perspective, we derive a series of magnetization and quantum spin current systems coupled via an "s-d" potential term, including the Schrödinger–Landau–Lifshitz–Maxwell system, the Pauli–Landau–Lifshitz system, and the Schrödinger–Landau–Lifshitz system with successive simplifications. For the latter two systems, we propose using the time splitting spectral method for the quantum spin current and the Gauss–Seidel projection method for the magnetization. Accuracy of the time splitting spectral method applied to the Pauli equation is analyzed and verified by numerous examples. Moreover, behaviors of the Schrödinger–Landau–Lifshitz system in different "s-d" coupling regimes are explored numerically.

Key words. Landau–Lifshitz equation, Schrödinger equation, Pauli equation, time splitting spectral method, variational structure

AMS subject classifications. 65M70, 78A25, 82C10

DOI. 10.1137/16M106947X

1. Introduction. Magnetic materials have been successfully used to record and store data for a long time. These materials produce their own persistent magnetic orders even in the absence of an external magnetic field. Magnetization is the vector field which describes the intrinsic magnetic order. Its dynamics was first modeled by Landau and Lifshitz in 1935 [18]. Even though the Landau–Lifshitz equation is a phenomenological model, it is still widely used in micromagnetics [4, 13]. While a rigorous microscopic derivation of the equation is still lacking, magnetization dynamics can be viewed as the collective dynamics of atomic magnetic moments.

In recent years, various techniques have been developed to ease magnetization reversal and switching; see [3, 14, 23] for examples and references therein. One effective way is to control the spin degrees of freedom (dofs) of electrons, which in turn affect the dynamics of magnetization. This is known as spin transfer torque (STT), observed independently by Fert [1] and Grünberg [11]. The presence of STT can reduce the characteristic time scale of data recording and storage processes by orders of magnitude. Models at different levels are proposed to understand magnetization dynamics in the presence of spin dofs. Numerous models have been developed to describe the dynamics of spin. One type of model adds an additional torque accounting for spin dynamics in the Landau–Lifshitz equation; see, for example, [8, 26]. The other type of model treats spin dynamics and magnetization dynamics on an equal footing; see, for example, [7, 22, 25]. In [25], linear response theory is used to derive a diffusion

*Received by the editors April 6, 2016; accepted for publication (in revised form) September 27, 2016; published electronically December 6, 2016.

http://www.siam.org/journals/mms/14-4/M106947.html

Funding: The first author acknowledges support from the Young Thousand Talents Program of China and National Natural Science Foundation of China via grant 21602149. The second author is partially supported by KI-Net NSF RNMS grant 1107291 and NSF grant DMS 1514826. The third author is partially supported by RNMS11-07444 (KI-Net).

†Mathematical Center for Interdisciplinary Research and School of Mathematical Sciences, Soochow University, Suzhou 215006, China (jingrunchen@suda.edu.cn).

‡Department of Mathematics and Department of Physics, Duke University, Box 90320, Durham NC 27708 (jliu@phy.duke.edu).

§Department of Mathematics, Duke University, Box 90320, Durham NC 27708 (zhennan@math.duke.edu).

equation for spin dynamics. A more microscopic justification for the diffusion-type equation is derived from the Boltzmann equation in [22]. Connections between these two types of models are made under certain assumptions [26].

In [7], a Schrödinger equation in the spinor form was used to model spin at the quantum level. Using the Wigner transform and moment closure, the authors derived a diffusion equation for spin dynamics. It recovers the model in [25] in the regime of weak spin-magnetization coupling. The model has been successfully used for magnetization switching [7] and domain wall dynamics [6] with both qualitative and quantitative agreements with experimental results. The passage from the Schrödinger equation to the diffusion equation relies on three main assumptions: (1) a BGK-type operator for the relaxation term in the Boltzmann equation; (2) certain moment closure to get a closed spin-magnetization coupled system; and (3) a quasi-static approximation to get the constitutive relation between the applied current density and the spin current density. These assumptions are difficult to verify except the last one, since its validity comes from the diffusive regime which can be checked from material constants.

Nevertheless, spin dynamics in the general case will be of great interest due to its universality. Therefore, we shall consider the Schrödinger equation in the spinor form and couple it to the Landau–Lifshitz equation. The purpose of the current paper is two-fold: (1) derive the coupled system and its analogue from a variational perspective (2) propose efficient algorithms for the coupled system and its analogue. In subsequent papers, we will analyze the variational models and show the existence of (weak) solutions. As a byproduct, we propose the time splitting spectral method for the Pauli equation, and rigorous convergence results are presented. This method has spectral accuracy in space and, in theory, high order temporal accuracy can be naturally achieved by the operator splitting method. It also allows large time steps to compute correct physical observables, which is ideal for hybrid simulation. The time splitting spectral method for the Pauli equation itself is of significance in terms of numerical analysis and scientific computations.

The rest of the paper is organized as follows. We derive the Schrödinger–Landau–Lifshitz–Maxwell system from a space-time total action, and the Pauli–Landau–Lifshitz system from a free energy formulation in section 2, where the Schrödinger–Landau–Lifshitz system can be considered as a simplified model of either case. In section 3, the time splitting spectral method for the Pauli equation is given analyzed in detail, and the Gauss–Seidel projection method of the Landau–Lifshitz equation is reviewed. Extensive numerical tests are provided in section 4, some of which are devoted to carefully verifying the numerical properties of the time splitting spectral method to the Pauli equation, while the rest are numerical examples of the Schrödinger–Landau–Lifshitz system in different coupling regimes.

2. Models and variational structures. In this section, we first describe the semiclassical spin dynamics by the Schrödinger equation in the spinor form coupled with the Landau–Lifshitz equation. The total space-time action is introduced to derive the Pauli–Landau–Lifshitz–Maxwell system and the Pauli–Landau–Lifshitz system is derived from construction of the free energy, whereas the Schrödinger–Landau–Lifshitz system can be viewed as a simplified model from each scenario.

2.1. The Schrödinger–Landau–Lifshitz system. For $\boldsymbol{x} \in \mathbb{R}^3$ and $t \in \mathbb{R}$, we denote the quantum wavefunction for spin $\pm\frac{1}{2}$ electrons by $\boldsymbol{\psi}(\boldsymbol{x}, t) \in \mathbb{C}^2$ and the magnetization by $\boldsymbol{m}(\boldsymbol{x}, t) \in \mathbb{R}^3$. The Schrödinger–Landau–Lifshitz system reads as

$$i\varepsilon\partial_t\boldsymbol{\psi}(\boldsymbol{x},t) = -\frac{\varepsilon^2}{2}\Delta_{\boldsymbol{x}}\boldsymbol{\psi}(\boldsymbol{x},t) + V(\boldsymbol{x})\boldsymbol{\psi}(\boldsymbol{x},t) - \eta\boldsymbol{m}(\boldsymbol{x},t)\cdot\hat{\sigma}\boldsymbol{\psi}(\boldsymbol{x},t), \quad \boldsymbol{x}\in\mathbb{R}^3, \tag{1}$$

$$\begin{aligned}\partial_t\boldsymbol{m}(\boldsymbol{x},t) &= -\boldsymbol{m}(\boldsymbol{x},t)\times(\boldsymbol{H}_{\text{eff}} + \eta\boldsymbol{s}(\boldsymbol{x},t))\\ &\quad - \alpha\boldsymbol{m}(\boldsymbol{x},t)\times(\boldsymbol{m}(\boldsymbol{x},t)\times(\boldsymbol{H}_{\text{eff}} + \eta\boldsymbol{s}(\boldsymbol{x},t))), \quad \boldsymbol{x}\in\Omega,\end{aligned} \tag{2}$$

$$\boldsymbol{\psi}(\boldsymbol{x},0) = \boldsymbol{\psi}_0(\boldsymbol{x}), \quad \boldsymbol{x}\in\mathbb{R}^3, \tag{3}$$

$$\boldsymbol{m}(\boldsymbol{x},0) = \boldsymbol{m}_0(\boldsymbol{x}), \quad \boldsymbol{x}\in\Omega. \tag{4}$$

Here Ω is the domain occupied by the magnetic material. The effective field $\boldsymbol{H}_{\text{eff}}$ has the form

$$\boldsymbol{H}_{\text{eff}} = \Delta\boldsymbol{m} - (m_2\boldsymbol{e}_2 + m_3\boldsymbol{e}_3) + (\boldsymbol{H}_{\text{s}} + \boldsymbol{H}_0) \tag{5}$$

and can be calculated as $-\frac{\delta F_{\text{LL}}}{\delta \boldsymbol{m}}$, where F_{LL} is the Landau–Lifshitz energy given by

$$F_{\text{LL}} = \frac{1}{2}\int_\Omega \left(m_2^2 + m_3^2\right) + \frac{1}{2}\int_\Omega |\nabla\boldsymbol{m}|^2 - \frac{1}{2}\int_\Omega \boldsymbol{H}_{\text{s}}\cdot\boldsymbol{m} - \int_\Omega \boldsymbol{H}_0\cdot\boldsymbol{m}. \tag{6}$$

Due to the presence of the spin density $\boldsymbol{s}$, it is natural to introduce the modified effective field

$$\tilde{\boldsymbol{H}}_{\text{eff}} = \boldsymbol{H}_{\text{eff}} + \eta\boldsymbol{s}. \tag{7}$$

In (5), $\{\boldsymbol{e}_j\}_{j=1}^3$ are the standard bases of $\mathbb{R}^3$. In (2), $\eta\boldsymbol{s}$ plays as an additional torque. $\boldsymbol{H}_0$ is the externally applied magnetic field and $\boldsymbol{H}_{\text{s}}$ is the stray field given by $\boldsymbol{H}_{\text{s}} = -\nabla U$, where U satisfies

$$U(\boldsymbol{x}) = \int_\Omega \nabla N(\boldsymbol{x}-\boldsymbol{y})\cdot\boldsymbol{m}(\boldsymbol{y},t)\,d\boldsymbol{y} \tag{8}$$

with $N(\boldsymbol{x}) = -1/(4\pi|\boldsymbol{x}|)$ denoting the Newtonian potential.

Here, (1) is the one-body Schrödinger equation, in which $\boldsymbol{\psi} = (\psi_+, \psi_-)^T$ is called the spinor, $\varepsilon\in(0,1]$ is the semiclassical parameter, $V(\boldsymbol{x})$ is the external scalar potential, and $\hat{\sigma} = \sigma_x\boldsymbol{e}_1 + \sigma_y\boldsymbol{e}_2 + \sigma_z\boldsymbol{e}_3$ gives the Pauli matrices

$$\sigma_x = \begin{pmatrix} 0 & 1\\ 1 & 0\end{pmatrix}, \quad \sigma_y = \begin{pmatrix} 0 & -i\\ i & 0\end{pmatrix}, \quad \sigma_z = \begin{pmatrix} 1 & 0\\ 0 & -1\end{pmatrix}.$$

The last term in the Hamiltonian of the Schrödinger equation describes the spin-magnetization interaction, i.e., the coupling between spin dofs of the applied current and magnetization. η is the corresponding coupling strength. This model neglects the self-induced electromagnetic fields generated by the applied current.

To extract macroscopic quantities, we define the density matrix

$$D = \boldsymbol{\psi}\boldsymbol{\psi}^\dagger = \begin{pmatrix} \psi_+\overline{\psi_+} & \psi_+\overline{\psi_-}\\ \psi_-\overline{\psi_+} & \psi_-\overline{\psi_-}\end{pmatrix},$$

then the associated position density ρ is defined as

$$\rho(\boldsymbol{x},t) = \text{Tr}\{D\} = \psi_+\overline{\psi_+} + \psi_-\overline{\psi_-}$$

and the spin density $\boldsymbol{s}$ is defined as

$$\boldsymbol{s}(\boldsymbol{x},t) = \text{Tr}\{D\hat{\sigma}\} = \text{Tr}\{D\sigma_x\}\boldsymbol{e}_1 + \text{Tr}\{D\sigma_y\}\boldsymbol{e}_2 + \text{Tr}\{D\sigma_z\}\boldsymbol{e}_3.$$

From (1), by direct calculation, the total mass of the quantum wavefunction, denoted by

$$\|\boldsymbol{\psi}\|(t) = \left(\int_{\mathbb{R}^3} |\psi_+(\boldsymbol{x},t)|^2 + |\psi_-(\boldsymbol{x},t)|^2 d\boldsymbol{x} \right)^{\frac{1}{2}},$$

is conserved, i.e.,

$$\frac{d}{dt}\|\boldsymbol{\psi}\| = 0.$$

As for the magnetization dynamics (2), the magnetization $\boldsymbol{m}(\boldsymbol{x},t)$ is normalized $|\boldsymbol{m}| = 1$ in the pointwise sense over Ω. A Neumann boundary condition is imposed for (2):

$$\frac{\partial \boldsymbol{m}}{\partial \nu} = 0 \quad \text{on} \quad \partial\Omega,$$

where ν is the unit normal vector on the domain boundary $\partial\Omega$.

By taking the inner product with $\boldsymbol{m}$, (2) becomes

$$\partial_t |\boldsymbol{m}|^2 = 0,$$

where we have used the fact that both terms on the right-hand side of (2) are perpendicular to $\boldsymbol{m}$. Hence, in the Schrödinger–Landau–Lifshitz system, both $\boldsymbol{\psi}$ and $\boldsymbol{m}$ stay normalized through time evolution. It is worth mentioning that the second term in (2) is known as the Gilbert damping [9], where $\alpha > 0$ is the damping constant.

This particular type of spin-magnetization interaction is the so-called "s-d" coupling model [7, 8], which is relatively well studied and widely used in the physics community. There are extensive experimental studies for many magnetic devices [14]. Other effects, such as the Rashba spin-orbit coupling and the Dzyaloshinskii–Moriya interaction, are also of great significance. These will also be considered in subsequent papers.

2.2. The total action and the Schrödinger–Landau–Lifshitz–Maxwell system. In this section, we aim to formulate the Schrödinger–Landau–Lifshitz–Maxwell system with the least action principle by constructing the total action. Previously, the variational structure of the Schrödinger equation has been widely known and well studied, and various Landau–Lifshitz models have been derived by the least action principle or the free energy approach (the reader may refer to [12] for a general discussion). However, the formulation becomes more challenging when the magnetic field is complicated, for example, when the self-induced electromagnetic field is considered, or when the external magnetic field is dominant. We aim to discuss these scenarios in the following, emphasizing their relations to the simplified Schrödinger–Landau–Lifshitz system.

For simplicity, we suppress the appearance of the parameters, since for the variation problem we only consider the case when all the parameters are fixed. In general, we consider the Schrödinger–Landau–Lifshitz–Maxwell action, which consists of the Schrödinger part S_{S}, the Landau–Lifshitz part S_{LL}, the Maxwell part S_{m}, and the spin-magnetization coupling part S_{C}:

$$S = S_{\mathrm{S}} + S_{\mathrm{LL}} + S_{\mathrm{m}} + S_{\mathrm{C}},$$

where

$$S_{\mathrm{S}} = \int_\Omega d\boldsymbol{x} \int dt \left[\mathrm{Re}\left(i\overline{\boldsymbol{\psi}} \frac{\partial \boldsymbol{\psi}}{\partial t} - \varphi |\boldsymbol{\psi}|^2 \right) - \frac{1}{2} \left| -i\nabla_{\boldsymbol{x}} \boldsymbol{\psi} - \mathbf{A}\boldsymbol{\psi} \right|^2 - V(\boldsymbol{x}) |\boldsymbol{\psi}|^2 \right],$$

$$S_{\mathrm{m}} = \int_{\mathbb{R}^3} d\boldsymbol{x} \int dt\, \frac{1}{2} \left(\left| \frac{\partial \mathbf{A}}{\partial t} + \nabla \varphi \right|^2 - |\nabla \times \mathbf{A} - \boldsymbol{m}|^2 \right),$$

$$S_{\mathrm{LL}} = -\int dt F_{LL},$$

and

$$S_{\mathrm{C}} = \int_{\Omega} d\boldsymbol{x} \int dt\, \boldsymbol{s} \cdot \boldsymbol{m}.$$

Note that S_{S}, S_{LL}, and S_{C} are defined on the material domain Ω, while S_{m} is defined on the whole space $\mathbb{R}^3$ since the electromagnetic field is induced even outside the material. Here $\mathbf{A}$ is the electromagnetic vector potential and φ is the self-induced scalar potential. To clarify the notation, we use

$$|-i\nabla_{\boldsymbol{x}} \boldsymbol{\psi} - \mathbf{A}\boldsymbol{\psi}|^2 = |-i\nabla_{\boldsymbol{x}} \psi_+ - \mathbf{A}\psi_+|^2 + |-i\nabla_{\boldsymbol{x}} \psi_- - \mathbf{A}\psi_-|^2,$$

which is a scalar. In the above expressions, S_{S} includes the time derivative contribution, the modified kinetic term, the electric scalar potential term, and the external potential term. S_{LL} describes the Landau–Lifshitz part. S_{m} includes the electric field contribution and the magnetic field contribution. S_{C} describes the coupling between the charged current and the magnetization of the ferromagnetic material by the "s-d" model.

In the absence of the Schrödinger equation, the action $S = S_{\mathrm{m}} + S_{\mathrm{LL}}$ with respect to φ, $\mathbf{A}$, and $\boldsymbol{m}$ gives the Landau–Lifshitz–Maxwell system; see [12]. With the presence of the polarized current described by the Schrödinger equation and due to the self-induced electromagnetic field, the vector potential modifies the quantum momentum operator by

$$-i\nabla \to -i\nabla - \mathbf{A},$$

which is referred to as the Peierls substitution [20, 21]. Also, the polarized current generates a spin density $\boldsymbol{s}$, which modifies the dynamics of the magnetization. For simplicity, we only keep a first order correction with respect to $\boldsymbol{s}$, given by S_{C}. In other words, S_{C} defines the interaction between the spin current and the magnetization in the system.

By taking variations with respect to $\boldsymbol{\psi}$, $\mathbf{A}$, φ, and $\mathbf{m}$, one can derive the coupled Schrödinger equation, the Maxwell equations, and the Landau–Lifshitz equation, respectively. Note that, although the vector potential $\mathbf{A}$ contains the partial contribution from the magnetization $\boldsymbol{m}$, we treat these two as independent variables.

The Schrödinger equation is obtained by the least action principle

$$\frac{\delta S}{\delta \overline{\boldsymbol{\psi}}} = \mathbf{0},$$

which leads to

$$i\partial_t \boldsymbol{\psi} = \frac{1}{2} \left(-i\nabla_{\boldsymbol{x}} - \mathbf{A}\right)^2 \boldsymbol{\psi} + (\varphi + V)\boldsymbol{\psi} - \boldsymbol{m}(\boldsymbol{x}, t) \cdot \hat{\sigma} \boldsymbol{\psi}(\boldsymbol{x}, t).$$

Next, to obtain the Maxwell equations, we consider the following two variational equations:

$$\frac{\delta S}{\delta \varphi} = 0, \quad \frac{\delta S}{\delta \mathbf{A}} = \mathbf{0}.$$

Then, we get

$$\nabla \cdot \left(\frac{\partial \mathbf{A}}{\partial t} + \nabla \varphi \right) = -\rho, \tag{9}$$

$$\nabla \times (\nabla \times \mathbf{A} - \boldsymbol{m}) + \frac{\partial}{\partial t} \left(\frac{\partial \mathbf{A}}{\partial t} + \nabla \varphi \right) = \mathbf{j}, \tag{10}$$

where

$$\mathbf{j} = \mathrm{Im}(\boldsymbol{\psi}^\dagger \nabla \boldsymbol{\psi}) - \mathbf{A}\rho$$

is the flux density.

We use the change of variables

$$\mathbf{E} = -\left(\frac{\partial \mathbf{A}}{\partial t} + \nabla \varphi \right),$$

$$\mathbf{B} = \nabla \times \mathbf{A}, \quad \mathbf{B} = \mathbf{H} + \mathbf{m}$$

and immediately get

$$\nabla \times \mathbf{E} + \partial_t \mathbf{B} = \mathbf{0}, \tag{11}$$

$$\nabla \cdot \mathbf{B} = 0. \tag{12}$$

Also, (9) and (10) can be written as

$$\nabla \cdot \mathbf{E} = \rho, \tag{13}$$

$$\nabla \times \mathbf{H} - \partial_t \mathbf{E} = \mathbf{j}. \tag{14}$$

Therefore, $\mathbf{E}$ and $\mathbf{B}$ can be interpreted, respectively, as the electric and the magnetic field. Equations (11), (12), (13), and (14) are precisely the Maxwell equations.

As in the original derivation of the Landau–Lifshitz equation, we cannot use the least action principle. Instead, we can first compute the modified effective field and then write the Landau–Lifshitz equation in the same way as in [18]:

$$\tilde{\boldsymbol{H}}_{\mathrm{eff}} = \frac{\delta S}{\delta \boldsymbol{m}}, \quad \partial_t \boldsymbol{m} = -\boldsymbol{m} \times \tilde{\boldsymbol{H}}_{\mathrm{eff}} - \alpha \boldsymbol{m} \times \big(\boldsymbol{m} \times \tilde{\boldsymbol{H}}_{\mathrm{eff}} \big).$$

2.3. Regarding the self-induced electromagnetic field. In general, in the absence of the external magnetic field, the $\mathbf{H}$ field has two sources: the self-induced field of the magnetization and the self-induced field by the charged current. In practice, the self-induced electromagnetic field can be neglected. In that case, the $\mathbf{H}$ field reduces to the stray field, or the demagnetization field, denoted by $\mathbf{H}_s$. The magnetic energy reduces to the stray field energy

$$\frac{1}{2} \int_{\mathbb{R}^3} d\boldsymbol{x} |\mathbf{H}_s|^2.$$

To clarify the relations between the magnetic field $\mathbf{B}$, the magnetization $\boldsymbol{m}$, and the stray field $\mathbf{H}_s$, we carry out the following heuristic arguments. Inside the ferromagnetic material, the magnetic field $\mathbf{B}$ consists of two parts:

$$\mathbf{B} = \mathbf{H}_s + \boldsymbol{m}. \tag{15}$$

But outside the material, the magnetic field $\mathbf{B}$ reduces to the stray field $\mathbf{H}_s$. By the Maxwell equations, we obtain that

$$\nabla \cdot \mathbf{B} = 0, \quad \nabla \times \mathbf{H}_s = \mathbf{0}. \tag{16}$$

The second equation implies $\mathbf{H}_s = -\nabla U$ for some scalar function U, often referred to as the magnetostatic potential. Then the first equation in (16) can be rewritten as

$$\nabla \cdot (-\nabla U + \mathbf{m}) = 0, \quad \boldsymbol{x} \in \mathbb{R}^3,$$

which shall be understood in the sense of distributions, i.e., $U \in H^1(\mathbb{R}^3)$ satisfies, for arbitrary test function $u \in H^1(\mathbb{R}^3)$,

$$\int_{\mathbb{R}^3} \nabla U \cdot \nabla u \, d\boldsymbol{x} = \int_{\Omega} \mathbf{m} \cdot \nabla u \, d\boldsymbol{x}. \tag{17}$$

This explains why the stray field $\mathbf{H}_s$ can be solved by solving the magnetostatic potential (8). The reader may refer to [4] for more details.

We want to point out that the formulation above can be viewed as the Helmholtz decomposition of the zero extension of the magnetization $\boldsymbol{m}$ to $\mathbb{R}^3$. With a bit of abuse of notation, we would still denote the extension of the magnetization by $\boldsymbol{m}$.

By Helmholtz's theorem, the vector field $\boldsymbol{m} : \mathbb{R}^3 \to \mathbb{R}^3$ can be resolved into the sum of an irrotational vector field and a divergence-free vector field

$$\boldsymbol{m} = \mathbf{B} - \mathbf{H}_s, \quad \nabla \cdot \mathbf{B} = 0, \quad \nabla \times \mathbf{H}_s = \mathbf{0}.$$

Due to the zero extension of the magnetization from Ω to $\mathbb{R}^3$, the decomposition has to be viewed in a weak sense, and the scalar potential of the divergence-free vector field is obtained by (17).

Moreover, with the curl-free part $\mathbf{H}_s$ defined in (17), the divergence-free part $\mathbf{B}$ is defined simultaneously by $\mathbf{B} = \boldsymbol{m} + \mathbf{H}_s$. One can easily check that the condition $\nabla \cdot \mathbf{B} = 0$ is satisfied automatically.

2.4. The free energy and the Pauli–Landau–Lifshitz system. In the previous part, we formulated the coupling model between the magnetization and the quantum spin density with interplay of the self-induced electromagnetic waves. In this section, we aim to explore a different scenario, that is, when the interaction between the magnetization and the quantum spin density is exposed to strong external electromagnetic fields.

In the presence of the external scalar potential V and the vector potential $\mathbf{A}$, we neglect the self-induced electromagnetic field, and consider the Pauli–Landau–Lifshitz free energy

$$\mathcal{F} = \int_{\Omega} \left[\frac{1}{2} \left| -i\nabla_{\boldsymbol{x}} \boldsymbol{\psi} - \mathbf{A}\boldsymbol{\psi} \right|^2 + V|\boldsymbol{\psi}|^2 - \boldsymbol{s} \cdot (\boldsymbol{m} + \mathbf{H}) \right] d\boldsymbol{x} + F_{\mathrm{LL}}. \tag{18}$$

In this formulation, the external electromagnetic field is dominant, and thus the scalar and vector potentials no longer satisfy the Maxwell equations. The free energy consists of the quantum kinetic energy, the quantum potential energy, the Landau–Lifshitz energy, and the spin magnetic field coupling energy.

Here, since the dominant magnetic field is treated as a prescribed function, the vector potential $\mathbf{A}$ itself is not considered an independent variable. The total magnetic field $\mathbf{B} = \nabla \times \mathbf{A} = \boldsymbol{m} + \mathbf{H}$ consists of the background magnetization $\boldsymbol{m}$ and the $\mathbf{H}$

field, where $\boldsymbol{m}$ is still an independent variable since its dynamics is governed by the Landau–Lifshitz equation. In theory, the $\mathbf{H}$ field includes the stray field and the external magnetic field, but we assume it is dominated by the external field, and we treat it as a given function. That is why we do not include the magnetic field energy in (18).

The Pauli (Schrödinger–Pauli) equation is obtained by

$$i\partial_t \boldsymbol{\psi} = \frac{\delta \mathcal{F}}{\delta \overline{\boldsymbol{\psi}}} = \frac{1}{2}\left(-i\nabla_{\boldsymbol{x}} + \mathbf{A}\right)^2 \boldsymbol{\psi} + V\boldsymbol{\psi} - \hat{\sigma}\cdot\mathbf{B}\boldsymbol{\psi}, \tag{19}$$

where $\hat{\sigma}\cdot\mathbf{B}\boldsymbol{\psi}$ is the so-called Stern–Gerlach term. Equivalently, we can write the Pauli equation as

$$i\partial_t \boldsymbol{\psi} = \frac{1}{2}\left(\hat{\sigma}\cdot\left(-i\nabla_{\boldsymbol{x}} + \mathbf{A}\right)\right)^2 \boldsymbol{\psi} + V\boldsymbol{\psi}.$$

In the Landau–Lifshitz equation, the modified effective field $\tilde{\boldsymbol{H}}_{\text{eff}}$ can be obtained in the same way as before, i.e., $\tilde{\boldsymbol{H}}_{\text{eff}} = -\frac{\delta \mathcal{F}}{\delta \boldsymbol{m}}$. Therefore, we have obtained the Pauli–Landau–Lifshitz system coupled by the spin magnetic field interaction.

2.5. The simplified model. So far, we have defined the total action which leads to the Schrödinger–Landau–Lifshitz–Maxwell system and the free energy which leads to the Pauli–Landau–Lifshitz system. To obtain the Schrödinger–Landau–Lifshitz system, we could either switch off the external magnetic field in the Pauli–Landau–Lifshitz system, i.e., reduce the spin magnetic field coupling energy to the spin-magnetization interaction energy, or we could neglect the self-induced electromagnetic field in the Schrödinger–Landau–Lifshitz–Maxwell system. We further explain the former approach in the following and the latter can be done in a similar fashion.

Assume that the self-induced electromagnetic field is negligible. The total energy functional of the Schrödinger–Landau–Lifshitz system simplifies to

$$\mathcal{F} = \int_\Omega \frac{1}{2}\left|-i\varepsilon\nabla_{\boldsymbol{x}}\boldsymbol{\psi}\right|^2 + V(\boldsymbol{x})|\boldsymbol{\psi}|^2 d\boldsymbol{x} + F_{\text{LL}} - \int_\Omega \eta \boldsymbol{s}\cdot\boldsymbol{m} d\boldsymbol{x}.$$

In other words, we only keep the kinetic and potential energy of the charged current, the Landau–Lifshitz energy, and the spin-magnetization coupling energy. Here, we have rescaled the quantum kinetic operator to $-i\varepsilon\nabla_{\boldsymbol{x}}$ for $\varepsilon \in (0,1]$. When $\varepsilon \ll 1$, the wavefunction of the charged current is in the highly oscillatory regime, which presents challenges both in analysis and computation. Also, the coupling strength η is included in the spin magnetic field coupling energy, which is an ad hoc parameter which may come from the procedure of nondimensionalization [6, 7].

Finally, we are ready to derive the system (1)–(2). Obviously, the effective field $\tilde{\boldsymbol{H}}_{\text{eff}}$ can be obtained by

$$\tilde{\boldsymbol{H}}_{\text{eff}} = -\frac{\delta \mathcal{F}}{\delta \boldsymbol{m}} = \boldsymbol{H}_{\text{eff}} + \eta \boldsymbol{s}.$$

Also, by direct calculation, the Schrödinger equation (1) can be rewritten as

$$i\varepsilon\partial_t \boldsymbol{\psi} = \frac{\delta \mathcal{F}}{\delta \overline{\boldsymbol{\psi}}} = \hat{H}\boldsymbol{\psi} = -\frac{\varepsilon^2}{2}\Delta_{\boldsymbol{x}}\boldsymbol{\psi}(\boldsymbol{x},t) + V(\boldsymbol{x})\boldsymbol{\psi}(\boldsymbol{x},t) - \eta\boldsymbol{m}(\boldsymbol{x},t)\cdot\hat{\sigma}\boldsymbol{\psi}(\boldsymbol{x},t).$$

Similarly, we have

$$i\varepsilon\partial_t \overline{\boldsymbol{\psi}} = \frac{\delta \mathcal{F}}{\delta \boldsymbol{\psi}} = \overline{\hat{H}}\,\overline{\boldsymbol{\psi}}.$$

Next, we show that the total energy $\mathcal{F}$ is nonincreasing in time. A straightforward calculation produces

$$\begin{aligned}\frac{d}{dt}\mathcal{F} &= \int_\Omega \left(\frac{\delta \mathcal{F}}{\delta \boldsymbol{\psi}} \cdot \partial_t \boldsymbol{\psi} + \frac{\delta \mathcal{F}}{\delta \overline{\boldsymbol{\psi}}} \cdot \partial_t \overline{\boldsymbol{\psi}} + \frac{\delta \mathcal{F}}{\delta \boldsymbol{m}} \cdot \partial_t \boldsymbol{m} \right) d\boldsymbol{x} \\ &= \int_\Omega \left(2\mathrm{Re}\left[\frac{\delta \mathcal{F}}{\delta \boldsymbol{\psi}} \cdot \partial_t \boldsymbol{\psi} \right] + \frac{\delta \mathcal{F}}{\delta \boldsymbol{m}} \cdot \partial_t \boldsymbol{m} \right) d\boldsymbol{x} \\ &= \int_\Omega \left(\frac{\delta \mathcal{F}}{\delta \boldsymbol{m}} \cdot \partial_t \boldsymbol{m} \right) d\boldsymbol{x}.\end{aligned}$$

In the last line, we use the fact that $\frac{\delta \mathcal{F}}{\delta \boldsymbol{\psi}} \cdot \partial_t \boldsymbol{\psi} = \frac{1}{i\varepsilon} |\hat{H}\boldsymbol{\psi}|^2$ is purely imaginary.

For the remaining term, we calculate that

$$\begin{aligned}\frac{\delta \mathcal{F}}{\delta \boldsymbol{m}} \cdot \partial_t \boldsymbol{m} &= -\tilde{H}_{\mathrm{eff}} \cdot \partial_t \boldsymbol{m} \\ &= \alpha \tilde{H}_{\mathrm{eff}} \cdot (\boldsymbol{m} \times (\boldsymbol{m} \times \tilde{H}_{\mathrm{eff}})) \\ &= \alpha (\boldsymbol{m} \times \tilde{H}_{\mathrm{eff}}) \cdot (\tilde{H}_{\mathrm{eff}} \times \boldsymbol{m}) \\ &= -\alpha \left| \boldsymbol{m} \times \tilde{H}_{\mathrm{eff}} \right|^2.\end{aligned}$$

Finally, we conclude that

$$\frac{d}{dt}\mathcal{F} = -\alpha \int_\Omega \left| \boldsymbol{m} \times \tilde{H}_{\mathrm{eff}} \right|^2 d\boldsymbol{x} \leqslant 0.$$

3. Numerical methods.

3.1. Time splitting spectral method for the Pauli equation. In the Schrödinger–Landau–Lifshitz system, the Schrödinger equation (1) can be considered as a simplified version of the Pauli equation (19), where the vector potential $\mathbf{A}$ vanishes and the magnetic field $\mathbf{B}$ reduces to the magnetization $\boldsymbol{m}$. In this section, we propose a time splitting spectral method (see [2, 15, 16, 19]) for the Pauli equation in the semiclassical regime

$$i\varepsilon \partial_t \boldsymbol{\psi} = \frac{1}{2} \left(-i\varepsilon \nabla_x + \mathbf{A} \right)^2 \boldsymbol{\psi} + V\boldsymbol{\psi} - \eta \hat{\sigma} \cdot \mathbf{B}\boldsymbol{\psi}, \tag{20}$$

where the vector potential $\mathbf{A}$ and the scalar potential V are prescribed functions, and the magnetic field $\mathbf{B}$ is given by

$$\mathbf{B} = \nabla \times \mathbf{A}. \tag{21}$$

For simplicity, we assume $\mathbf{A}$ and V are time-independent functions. The extension to time-dependent potential cases is straightforward.

Here, the coefficient η defines the strength of the Stern–Gerlach term, which is reminiscent of the "s-d" coupling strength in the Schrödinger–Landau–Lifshitz system. We aim to design a numerical method for the system for wide ranges of parameters ε and η. In particular, the method should work for the semiclassical regime, namely, $\varepsilon \ll 1$ and for the strong coupling regime, namely, $\eta = O(1)$.

Without loss of generality, we assume the Coulomb gauge $\nabla \cdot \mathbf{A} = 0$; the Pauli equation can be formulated as

$$i\varepsilon \partial_t \boldsymbol{\psi} = -\frac{\varepsilon^2}{2} \Delta \boldsymbol{\psi} + i\varepsilon A \cdot \nabla \boldsymbol{\psi} + \left(\frac{1}{2} |\mathbf{A}|^2 + V - \eta \hat{\sigma} \cdot \mathbf{B} \right) \boldsymbol{\psi}. \tag{22}$$

By the operator splitting technique, for every time step $t \in [t_n, t_{n+1}]$, one solves the kinetic step

$$i\varepsilon\partial_t \boldsymbol{\psi} = -\frac{\varepsilon^2}{2}\Delta\boldsymbol{\psi}, \quad t \in [t_n, t_{n+1}], \tag{23}$$

followed by the potential step

$$i\varepsilon\partial_t \boldsymbol{\psi} = \left(\frac{1}{2}|\mathbf{A}|^2 + V - \eta\hat{\sigma}\cdot\mathbf{B}\right)\boldsymbol{\psi}, \quad t \in [t_n, t_{n+1}], \tag{24}$$

and followed by the convection step

$$\partial_t \boldsymbol{\psi} = \mathbf{A}\cdot\nabla\boldsymbol{\psi}, \quad t \in [t_n, t_{n+1}]. \tag{25}$$

For clarity, we rewrite the equation as

$$\partial_t \boldsymbol{\psi} = (\mathcal{A} + \mathcal{B} + \mathcal{C})\,\boldsymbol{\psi}, \tag{26}$$

where

$$\mathcal{A} = \frac{i\varepsilon}{2}\Delta, \quad \mathcal{B} = -\frac{i}{\varepsilon}\left(\frac{1}{2}|\mathbf{A}|^2 + V - \eta\hat{\sigma}\cdot\mathbf{B}\right), \quad \text{and} \quad \mathcal{C} = \mathbf{A}\cdot\nabla.$$

For simplicity, we consider the Pauli equation in one dimension with periodic boundary conditions. The extension to multidimensional cases is straightforward. In the one-dimensional case, the vector potential $\mathbf{A}$ reduces to a scalar function, so the relation (21) is no longer satisfied. Hence, to demonstrate the construction of the numerical method, we suppose $\mathbf{B}$ to be a three-component vector which is independent of $\mathbf{A}$.

We assume, on computation domain $[a, b]$, a uniform spatial grid $x_j = a + j\Delta x$, $j = 0, \ldots, N-1$, where $N = 2^{n_0}$, n_0 is a positive integer, and $\Delta x = \frac{b-a}{N}$. We also assume uniform time steps $t_k = k\Delta t$, $k = 0, \ldots, K$. The construction of numerical methods is based on the following (first order) operator splitting technique.

Let $\boldsymbol{\psi}(t_n)$ be the exact solution at $t = t_n$, which implies

$$\boldsymbol{\psi}(t_{n+1}) = e^{(\mathcal{A}+\mathcal{B}+\mathcal{C})\Delta t}\boldsymbol{\psi}(t_n).$$

Let $\boldsymbol{\psi}_j^n$ be the numerical approximation of $\boldsymbol{\psi}(x_j, t_n)$ and let $\boldsymbol{\psi}^n$ be the numerical approximation of $\boldsymbol{\psi}(t_n)$, which means $\boldsymbol{\psi}^n$ has $\boldsymbol{\psi}_j^n$ as its components.

Define the solution obtained by the (first order) operator splitting (without spatial discretization) as

$$w^{n+1} = e^{\mathcal{C}\Delta t}e^{\mathcal{B}\Delta t}e^{\mathcal{A}\Delta t}\boldsymbol{\psi}(t_n). \tag{27}$$

Note that w^{n+1} differs from $\boldsymbol{\psi}(t_{n+1})$ due to the operator splitting error.

After operator splitting, the kinetic step can be solved analytically in time in the Fourier space:

$$\boldsymbol{\psi}_j^* = \frac{1}{N}\sum_{l=-N/2}^{N/2-1} e^{-i\varepsilon\Delta t\mu_l^2/2}\hat{\boldsymbol{\psi}}_l^n e^{i\mu_l(x_j-a)}, \tag{28}$$

where $\hat{\boldsymbol{\psi}}_l^n$ are Fourier coefficients of $\boldsymbol{\psi}_j^n$ defined by

$$\hat{\boldsymbol{\psi}}_l^n = \sum_{j=0}^{N-1} \boldsymbol{\psi}_j^n e^{-i\mu_l(x_j-a)}, \quad \mu_l = \frac{2\pi l}{b-a}, \quad l = -\frac{M}{2}, \ldots, \frac{M}{2} - 1.$$

For the potential step, due to the presence of $\hat{\sigma} \cdot \mathbf{B}$, the whole potential is a 2×2 matrix. Fortunately, we have the following identity for the exponential of Pauli matrices, for any $\vec{a} = a\hat{n}$, $|\hat{n}| = 1$:

$$e^{ia(\hat{n}\cdot\hat{\sigma})} = I \cos a + i(\hat{n} \cdot \hat{\sigma}) \sin a,$$

which is analogous to Euler's formula. I is the 2×2 identity matrix. Thus, by the method of integration factor, we can derive the explicit solution of the potential step:

(29)
$$\boldsymbol{\psi}_j^{**} = \exp\left(-\frac{i\Delta t}{\varepsilon}\left(\frac{1}{2}|\mathbf{A}_j|^2 + V_j\right)\right)\left(I\cos\left(\frac{\Delta t\eta|\mathbf{B}_j|}{\varepsilon}\right) + i(\hat{\mathbf{B}}_j \cdot \hat{\sigma})\sin\left(\frac{\Delta t\eta|\mathbf{B}_j|}{\varepsilon}\right)\right)\boldsymbol{\psi}_j^*.$$

Here, we denote

$$\mathbf{A}(x_j) = \mathbf{A}_j, \quad \mathbf{B}(x_j) = \mathbf{B}_j = |\mathbf{B}_j|\hat{\mathbf{B}}_j, \quad \text{and} \quad V(x_j) = V_j.$$

Since we have used the analytical solutions in the kinetic step and in the potential step, there is no numerical error in time discretization of these two substeps.

In general, if we consider the potential step with a time-independent Hermitian matrix potential $\mathbf{M}$, we have

(30)
$$i\varepsilon\partial_t\boldsymbol{\psi} = \mathbf{M}\boldsymbol{\psi}, \quad t \in [t_n, t_{n+1}].$$

In particular, we can obviously check that $\frac{1}{2}|\mathbf{A}|^2 + V - \eta\hat{\sigma} \cdot \mathbf{B}$ is Hermitian. Moreover, we express the analytical solution as

$$\boldsymbol{\psi}(t_{n+1}) = \exp\left(-\frac{i\mathbf{M}\Delta t}{\varepsilon}\right)\boldsymbol{\psi}(t_n).$$

Numerically, this matrix exponential can be computed by the eigenvalue decomposition with minimal error. However, in the Pauli equation, or when the matrix potential consists of the Pauli matrices, the analytical expression (29) is superior in both efficiency and accuracy.

For the convection step, however, there is no obvious way to solve it analytically based on discrete data for a variable $\mathbf{A}(x)$. We propose a semi-Lagrangian method to solve the convection equation (25) as in [16, 19].

This method consists of two parts: backward characteristic tracing and interpolation. We compute the data $\boldsymbol{\psi}_j^{n+1}$ by first tracing backwards along the characteristic line

(31)
$$\frac{dx(t)}{dt} = -\mathbf{A}\left(x(t)\right), \quad x(t_{n+1}) = x_j,$$

for time interval $[t_n, t_{n+1}]$. Denote $x(t_n) = x_j^0$, obtained by numerically solving the ODE (31) backwards in time as shown in Figure 1.

We call the point set $\{x_j^0\}$ the shifted point set. By the method of characteristics, $\boldsymbol{\psi}_j^{n+1} = \boldsymbol{\psi}^{**}\left(x_j^0\right)$. But $\boldsymbol{\psi}^{**}\left(x_j^0\right)$ in general are not known, since x_j^0 are not necessarily

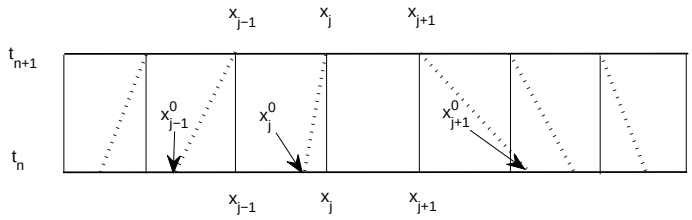

FIG. 1. *Backward tracing: x_j are the grid points; x_j^0 are the shifted grid points, which are the solutions to problem* (31) *backwards in time at $t = t_n$; and the dotted line indicates characteristics.*

grid points. Therefore, interpolation is needed to approximate $\boldsymbol{\psi}_j^{n+1} = \boldsymbol{\psi}^{**}\left(x_j^0\right)$ based on $\boldsymbol{\psi}^{**}$. We compare the following two choices: the spectral interpolation and the Mth order polynomial interpolation.

For the spectral approximation, the interpolant $\Pi_N \boldsymbol{\psi}^{**}(x) = \sum_{k=-N/2}^{N/2-1} c_k e^{ikx}$ is a global approximation to $\boldsymbol{\psi}^{**}(x)$ based on $\boldsymbol{\psi}^{**}$. One needs $O(N\log N)$ operations to get the Fourier coefficients c_k via the FFT method. But one needs $O(N)$ operations to evaluate the interpolant at each point x_j^0, since the shifted points x_j^0 are not necessarily the grid points, which means the inverse FFT does not apply. Hence, the total cost is $O(N^2)$ in each time step. This will make the whole scheme very costly. However, one can make use of the recently developed methodology nonuniform FFT (NUFFT) (see [10]) to implement this interpolation with $O(N\log N)$ cost. The details of this implementation and the corresponding stability analysis have been given in [19].

For the Mth order Lagrange polynomial interpolation, one needs to establish a polynomial interpolant for each shifted point x_j^0 with the discrete data on the closest M grid points $x_{j_1}, \ldots, x_{j_M}$. For each shifted point x_j^0, one uses M grid points near x_j^0 to form a Lagrange polynomial interpolant to approximate $U(x_j^0)$ with error of order $O(\Delta x^M)$. But certain stability constraints need to be satisfied for different interpolation methods. The extensive stability study of this method has been carried out in [16]. The total cost of the semi-Lagrangian method with the polynomial interpolation is $O(N)$ for each time step.

By either interpolation option, we have shown that the method for the convection step is unconditionally stable. In the following, we continue our analysis with the spectral interpolation option. The analysis with polynomial interpolations can be carried out in a similar fashion. For simplicity, we name this method the first order time splitting spectral (TSSP) method.

We conclude this section with the following remark.

Remark 3.1. The first order operator splitting implies first order convergence in time. One can make use of Strang's splitting to obtain a second order time discretization method. If one wants to apply the second order Strang's splitting to three operators, one can first group $\mathcal{A} + \mathcal{B}$ together as a single operator, and then apply Strang's splitting to $\mathcal{A}+\mathcal{B}$ and $\mathcal{C}$, while in the steps corresponding to $\mathcal{A}+\mathcal{B}$, one also uses Strang's splitting.

3.2. Error analysis of the TSSP method. To analyze the convergence of the TSSP method for the Pauli equation, it is worth noting that the Pauli equation and the Schrödinger equation with vector potential share many similarities. The TSSP

method for the Schrödinger equation has been analyzed in [16, 19], so we will only highlight the differences.

We further assume that the wavefunctions are ε-oscillatory in space and time but the potentials are not oscillatory. So there are t, ε, x independent positive constants C_m that

$$\left\| \frac{\partial^{m_1+m_2}}{\partial x^{m_1}\partial t^{m_2}} \boldsymbol{\psi}_{\pm}(t,\cdot) \right\|_{C([0,T];L^2(a,b))} \leqslant \frac{1}{\varepsilon^{m_1+m_2}} C_{m_1+m_2}, \tag{32}$$

$$\left\| \frac{\partial^m}{\partial x^m} \mathbf{A} \right\|_{L^2(a,b)} \leqslant C_m, \quad \left\| \frac{\partial^m}{\partial x^m} V \right\|_{L^2(a,b)} \leqslant C_m \tag{33}$$

$$\left\| \frac{\partial^m}{\partial x^m} \mathbf{B}_l \right\|_{L^2(a,b)} \leqslant C_m, \quad l = 1,2,3. \tag{34}$$

Note that the differentiation operator is unbounded for general smooth functions, but it is bounded in the subspace of smooth L^2 functions which are at most ε-oscillatory.

Since in the Pauli equation there is the additional Stern–Gerlach term, we need to study the resulting error in the operator splitting. We show, by studying the commutators between the three operators in (26), when the potentials are spatially variant, that the local splitting error in the first order splitting (23)–(25) for (22) is

$$\boldsymbol{\psi}(t_{n+1}) - w^{n+1} = \boldsymbol{\psi}(t_{n+1}) - e^{\mathcal{C}\Delta t} e^{\mathcal{B}\Delta t} e^{\mathcal{A}\Delta t} \boldsymbol{\psi}(t_n) = O\left(\frac{\Delta t^2}{\varepsilon}\right). \tag{35}$$

Clearly, the exact solution to (22) at $t = t_{n+1}$ with initial data $\boldsymbol{\psi}(t_n)$ is given by

$$\boldsymbol{\psi}(t_{n+1}) = e^{(\mathcal{A}+\mathcal{B}+\mathcal{C})\Delta t} \boldsymbol{\psi}(t_n).$$

The operator splitting error results from the noncommutativity of the operators $\mathcal{A}$, $\mathcal{B}$, and $\mathcal{C}$. In previous literature (see [2, 16]), the commutator was analyzed for scalar Schrödinger equations. The Pauli equation, on the other hand, is in the vector form, whereas the kinetic part $\mathcal{A}$ and the convection part $\mathcal{C}$ are still scalar operators. But in the potential part, due to the presence of $\hat{\sigma}\cdot\mathbf{B}$, the total potential is in a Hermitian matrix. As in [16, 19], it was shown that

$$[\mathcal{A}\Delta t, \mathcal{C}\Delta t]\boldsymbol{\psi} = O\left(\frac{\Delta t^2}{\varepsilon}\right),$$

where $[\cdot,\cdot]$ denotes the commutator. Direct computation gives

$$[\mathcal{A}\Delta t, \mathcal{B}\Delta t]\boldsymbol{\psi} = (\Delta t)^2 \left[\frac{1}{2}(\Delta_x \mathbf{M}) + \frac{1}{2}\partial_x \mathbf{M} \partial_x\right] \boldsymbol{\psi} = O\left(\frac{\Delta t^2}{\varepsilon}\right),$$

$$[\mathcal{B}\Delta t, \mathcal{C}\Delta t]\boldsymbol{\psi} = (\Delta t)^2 \left(-\frac{i}{\varepsilon}\right) (\mathbf{A}\partial_x \mathbf{M})\, \boldsymbol{\psi} = O\left(\frac{\Delta t^2}{\varepsilon}\right),$$

where again we denote

$$\mathbf{M} = \frac{1}{2}|\mathbf{A}|^2 + V - \eta\hat{\sigma}\cdot\mathbf{B}.$$

Therefore, we have formally shown that the local operator splitting error is $O(\frac{\Delta t^2}{\varepsilon})$ as in (35). Actually, the proof can be made completely rigorous if we give more assumptions on the wavefunction and the potentials similar to those in [2, 16, 19].

We use f_I to denote the spectral approximation based on the discrete data f_j or $f(x_j)$. Now we are ready to state the following error estimate for the first order TSSP method. The proof will be very similar to those in [2, 16, 19], except for the splitting error analysis which we have presented. Therefore, we would like to omit the proof.

THEOREM 3.1. *Let $\boldsymbol{\psi}(t,x)$ be the exact solution of* (22) *and let $\boldsymbol{\psi}^n$ be the discrete approximation by the first order TSSP method. We assume that the characteristic equations* (31) *are numerically solved with minimal error in the preprocessed step, and that the spectral interpolation with the NUFFT technique is taken in the semi-Lagrangian method for the convection step, where the extra error introduced by NUFFT is negligible. Under assumption* (34)*, we further assume $\Delta x/\varepsilon = O(1)$ and $\Delta t/\varepsilon = O(1)$; then, for all positive integers $m \geqslant 1$ and $t \in [0,T]$,*

$$||\boldsymbol{\psi}(t_n) - \boldsymbol{\psi}_I^n||_{L^2} \leqslant G_m \frac{T}{\Delta t}\left(\frac{\Delta x}{\varepsilon}\right)^m + \frac{CT\Delta t}{\varepsilon}, \tag{36}$$

where C is a positive constant independent of Δt, Δx, ε, m, and M, and G_m are positive constants independent of Δt, Δx, and ε.

3.3. Review of the Gauss–Seidel projection method for the Landau–Lifshitz equation. For the purpose of numerical simulation, we describe the Gauss–Seidel projection method for the Landau–Lifshitz equation, which was originally introduced by Wang, García-Cervera, and E in [24]. Here, we present a brief review of this method for completeness.

Consider the Landau–Lifshitz equation

$$\begin{aligned}\partial_t \mathbf{m}(x,t) = &-\mathbf{m}(x,t)\times(\Delta_x\mathbf{m}(x,t) + f(\mathbf{m},t))\\ &-\alpha\mathbf{m}(x,t)\times(\mathbf{m}(x,t)\times(\Delta_x\mathbf{m}(x,t) + f(\mathbf{m},t)))\end{aligned} \tag{37}$$

with

$$f(\mathbf{m},t) = H_{\text{eff}} - \Delta_x\mathbf{m}(x,t) + \eta\mathbf{s}(x,t).$$

Given $\mathbf{m}^n$ and $\mathbf{s}^n$, it solves (37) in three steps.

1. Implicit Gauss-Seidel step:

$$g_i^n = (I - \Delta t\Delta_h)^{-1}(m_i^n + \Delta t f_i^n), \tag{38}$$

$$g_i^* = (I - \Delta t\Delta_h)^{-1}(m_i^* + \Delta t f_i^*), \quad i = 1,2,3, \tag{39}$$

$$\begin{pmatrix} m_1^* \\ m_2^* \\ m_3^* \end{pmatrix} = \begin{pmatrix} m_1^n + (g_2^n m_3^n - g_3^n m_2^n) \\ m_2^n + (g_3^n m_1^* - g_1^* m_3^n) \\ m_3^n + (g_1^* m_2^* - g_2^* m_1^*) \end{pmatrix}, \tag{40}$$

   where $f_i^n = f_i(\mathbf{m}^n, \mathbf{s}^n)$ and $f_i^* = f_i(\mathbf{m}^*, \mathbf{s}^n)$, i.e., the most current values for $\mathbf{m}$ are used in f^*. Note that the value of $\mathbf{s}$ is frozen at $t = t_n$.

2. Heat flow without constraints:

$$\begin{pmatrix} m_1^{**} \\ m_2^{**} \\ m_3^{**} \end{pmatrix} = \begin{pmatrix} m_1^* + \alpha\Delta t(\Delta_h m_1^{**} + f_1^*) \\ m_2^* + \alpha\Delta t(\Delta_h m_2^{**} + f_2^*) \\ m_3^* + \alpha\Delta t(\Delta_h m_3^{**} + f_3^*) \end{pmatrix}. \tag{41}$$

3. Projection onto S^2:

$$\begin{pmatrix} m_1^{n+1} \\ m_2^{n+1} \\ m_3^{n+1} \end{pmatrix} = \frac{1}{|m^{**}|} \begin{pmatrix} m_1^{**} \\ m_2^{**} \\ m_3^{**} \end{pmatrix}. \tag{42}$$

The Gauss–Seidel projection method is stable and has first order accuracy in time. Even though it is an implicit method, it only requires solving linear systems of equations of the heat-equation type with constant coefficients, and thus is computationally much cheaper than other implicit methods for the Landau–Lifshitz equation, such as the backward Euler method.

3.4. Discussion on the numerical method for the coupled model. In the previous sections, we respectively established the TSSP method for the Pauli equation and reviewed the Gauss–Seidel projection method for the Landau–Lifshitz equation. In section, we combine these two methods and apply them to the Schrödinger–Landau–Lifshitz system (1)–(2). The Pauli–Landau–Lifshitz system can be solved in a similar way.

From time step t_n to t_{n+1}, we first freeze the coupling terms on the right-hand side of each equation to t_n, which is a first order approximation in time, and the continuous model is given by

$$i\varepsilon\partial_t\boldsymbol{\psi}(\boldsymbol{x},t) = -\frac{\varepsilon^2}{2}\Delta_{\boldsymbol{x}}\boldsymbol{\psi}(\boldsymbol{x},t) + V(\boldsymbol{x})\boldsymbol{\psi}(\boldsymbol{x},t) - \eta\boldsymbol{m}_I^n(\boldsymbol{x})\cdot\hat{\sigma}\boldsymbol{\psi}(\boldsymbol{x},t), \tag{43}$$

$$\begin{aligned}\partial_t\boldsymbol{m}(\boldsymbol{x},t) &= -\boldsymbol{m}(\boldsymbol{x},t)\times(\boldsymbol{H}_{\text{eff}} + \eta\boldsymbol{s}_I^n(\boldsymbol{x})) \\ &\quad - \alpha\boldsymbol{m}(\boldsymbol{x},t)\times(\boldsymbol{m}(\boldsymbol{x},t)\times(\boldsymbol{H}_{\text{eff}} + \eta\boldsymbol{s}_I^n(\boldsymbol{x}))),\end{aligned} \tag{44}$$

$$\boldsymbol{\psi}(\boldsymbol{x},t_n) = \boldsymbol{\psi}_I^n(\boldsymbol{x}), \quad \boldsymbol{m}(\boldsymbol{x},t_n) = \boldsymbol{m}_I^n(\boldsymbol{x}). \tag{45}$$

Here, $\mathbf{m}_I^n(\boldsymbol{x})$ is the interpolation function based on $\boldsymbol{m}_j^n$, $\boldsymbol{\psi}_I^n(\boldsymbol{x})$ is the spectral interpolation function base on $\boldsymbol{\psi}_j^n$, and $\boldsymbol{s}_I^n(\boldsymbol{x})$ is the spin density of $\boldsymbol{\psi}_I^n(\boldsymbol{x})$. Then, we apply the TSSP method to (43) to obtain $\boldsymbol{\psi}_j^{n+1}$, and the Gauss–Seidel projection method for (44) to get $\boldsymbol{m}_j^{n+1}$.

In this paper, we do not focus on rigorous numerical analysis of the combined method for this system, nor do we aim for high accuracy schemes. Instead, we would like to numerically understand the physical significance of the coupling mechanism. We conclude this section with some remarks.

Remark 3.2. This combined scheme is first order accurate in time because the coupling term is treated explicitly and the method for each equation is first order accurate in time. In principle, the coupling terms can be approximated with better accuracy (for example, extrapolation) and the Schrödinger equation can be solved with the high order operator splitting method. However, it is highly nontrivial to improve the accuracy of the Gauss–Seidel projection method in time. This is one of the possible future directions we could work on.

Remark 3.3. For the first order approximate system (43)–(44), since the TSSP method and the Gauss–Seidel projection method have different accuracies, we can apply different spatial meshes and time steps for each equation. Roughly speaking, due to the high oscillatory nature of the wavefunction to the Schrödinger equation, we can apply finer time steps and resolved spatial meshes in the TSSP method, while we can take ε-independent time steps and spatial meshes in the Gauss–Seidel projection method. Actually, we show in Example 4.1 that, even when the coupling strength

$\eta = 1$, the TSSP method is able to capture the correct physical observables with ε-independent Δt. Also, we show in Example 4.2, providing the snapshots of the position density and the spin density, that, while the wavefunctions are highly oscillatory, the physical observables are rather smooth. So far, the mesh sizes for the Schrödinger equation and the Landau–Lifshitz equation are still chosen empirically. The optimal choice of the mesh sizes is an interesting topic, which we may explore in the future.

Remark 3.4. It has been well understood that for many types of Schrödinger equations [2, 15, 16, 19], one can take ε-independent time steps to capture the correct physical observables, which are a macroscopic quantity associated with the wavefunction. The analysis requires an understanding of the semiclassical limit of the Schrödinger equation in the framework of Wigner transforms. However, the semiclassical equation of this model is only partially understood. The reader may refer to Chai's recent work on the semiclassical limit when the coupling strength $\eta = O(\varepsilon)$ [5]. In this paper, we shall test only numerically whether this feature extends to the Pauli equation in the next section.

4. Numerical examples.

4.1. The Pauli equation. In this section, we test the TSSP method for the Pauli equation in one dimension and in two dimensions. In the one-dimensional test, we examine the numerical convergence in time step and spatial mesh size, respectively. In the two-dimensional test, some snapshots of the wavefunctions and related physical observables are presented to demonstrate the accuracy of this method.

Also, we numerically investigate whether we can take ε independent of time steps to capture the correct physical observables. This property is a well-studied feature of TSSP methods applied to most linear and some nonlinear Schrödinger equations by the semiclassical analysis of the related Wigner transforms; see [2, 16]. However, the semiclassical limit of the Pauli equation in the framework of Wigner transforms is not yet well understood. It is worth pointing out that a recent work by Chai, García–Cervera, and Yang [5] has rigorously justified the semiclassical limit of a Schrödinger–Landau–Lifshitz system in the weak coupling regime, namely, the coupling strength $\eta = O(\varepsilon)$. This implies that at least when $\eta = O(\varepsilon)$, ε-independent time steps are allowed to compute the correct physical observables.

Example 4.1. In this example, we aim to carry out extensive numerical tests to verify the properties of the TSSP method applied to the Pauli equation in one dimension. We choose the following WKB-type initial condition:

$$\psi_+(x,0) = \psi_-(x,0) = \exp\left(i\frac{x}{2\varepsilon}\right)\exp\left(-32\left(x-\frac{1}{2}\right)^2\right).$$

Roughly speaking, this initial condition denotes a semiclassical spinor localized around $x = \frac{1}{2}$ moving with speed $\frac{1}{2}$. We choose the computation domain to be $[-\pi, \pi]$ so that periodic conditions can be imposed with negligible error. We also choose the following potentials and magnetic field:

$$V = \frac{x^2}{2}, \quad \mathbf{A} = \frac{\cos(x)}{2}, \quad \mathbf{B} = (\sin(x), \cos(x), 1).$$

Again, in one dimension, the Pauli equation is just a test model and no relation between $\mathbf{A}$ and $\mathbf{B}$ is assumed. Unless specified, the coupling strength η is set to be 1.

In this first test, we numerically verify that the proposed method has spectral convergence in spatial mesh size Δx. For $\varepsilon = \frac{1}{128}$ and $\frac{1}{512}$, we use the TSSP method

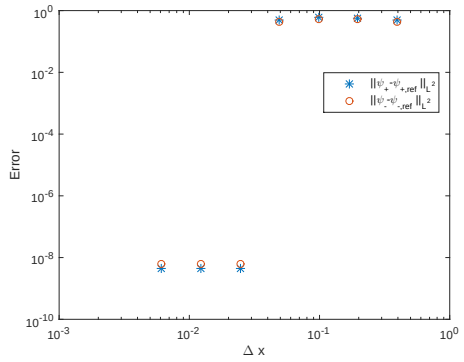

(a) $\varepsilon = \frac{1}{128}$

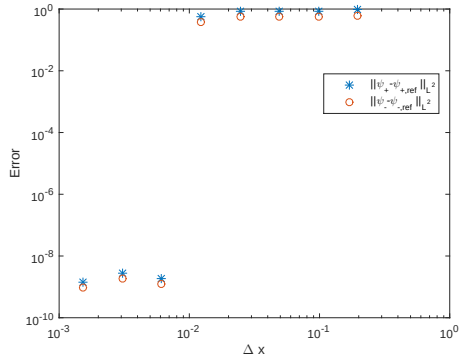

(b) $\varepsilon = \frac{1}{512}$

FIG. 2. *Spatial convergence tests.* (a) $\varepsilon = \frac{1}{128}$, $\Delta t = \frac{0.4\varepsilon}{128}$, $\Delta x = \frac{2\pi}{16}$, $\frac{2\pi}{32}$, $\frac{2\pi}{64}$, $\frac{2\pi}{128}$, $\frac{2\pi}{256}$, $\frac{2\pi}{512}$, *and* $\frac{2\pi}{1024}$. (b) $\varepsilon = \frac{1}{512}$, $\Delta t = \frac{0.4\varepsilon}{128}$, $\Delta x = \frac{2\pi}{32}$, $\frac{2\pi}{64}$, $\frac{2\pi}{128}$, $\frac{2\pi}{256}$, $\frac{2\pi}{512}$, $\frac{2\pi}{1024}$, $\frac{2\pi}{2048}$, *and* $\frac{2\pi}{4096}$.

to compute up to $t = 0.4$ with sufficiently fine time step $\Delta t = \frac{0.4\varepsilon}{128}$ and various spatial mesh sizes Δx. Due to the lack of analytical solutions, the reference solutions are computed with sufficiently fine mesh strategy

$$\Delta t = \frac{0.4\varepsilon}{128}, \quad \Delta x = \frac{2\pi\varepsilon}{128}. \tag{46}$$

The numerical results are plotted in Figure 2, from which we can confirm that when $\Delta x = O(\varepsilon)$, the numerical error converges spectrally. Note that due to the use of the NUFFT algorithm in the convection step (see [10]), the numerical error is not minimal when $\Delta x = O(\varepsilon)$. But, ideally, the convergence in Δx is spectral.

Second, we test the convergence in time steps, which is first order accurate. We fix $\varepsilon = \frac{1}{128}$ and $\varepsilon = \frac{1}{512}$, and for various Δt and sufficiently small Δx, we compute the solutions at $t = 0.4$. The reference solutions are computed with sufficiently small meshes (46). The errors in the wavefunctions, the position density, and the spin density are plotted in Figure 3, which clearly confirms the first order accuracy.

Finally, we test whether we can use ε-independent Δt to compute correct physical observables. We first fix the coupling strength $\eta = \varepsilon$ and time step $\Delta t = \frac{1}{25}$. For variant ε, we use the resolved spatial mesh to compute the Pauli equation up to $t = 0.4$. The reference solutions are computed with sufficiently small meshes (46).

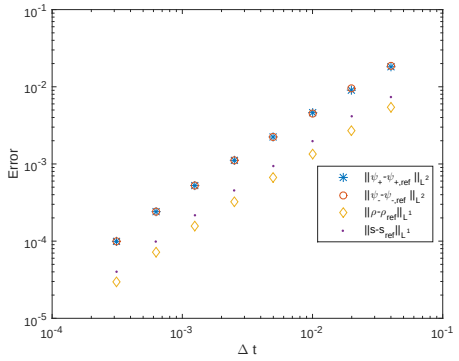

(a) $\varepsilon = \frac{1}{128}$

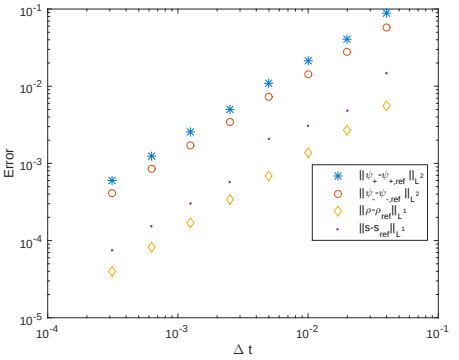

(b) $\varepsilon = \frac{1}{512}$

FIG. 3. *Temporal convergence tests.* (a): $\varepsilon = \frac{1}{128}$, $\Delta x = \frac{2\pi\varepsilon}{128}$, $\Delta t = \frac{1}{25}$, $\frac{1}{50}$, $\frac{1}{100}$, $\frac{1}{200}$, $\frac{1}{400}$, $\frac{1}{800}$, $\frac{1}{1600}$, *and* $\frac{1}{3200}$. (b) $\varepsilon = \frac{1}{512}$, $\Delta x = \frac{2\pi\varepsilon}{128}$, $\Delta t = \frac{1}{25}$, $\frac{1}{50}$, $\frac{1}{100}$, $\frac{1}{200}$, $\frac{1}{400}$, $\frac{1}{800}$, $\frac{1}{1600}$, *and* $\frac{1}{3200}$.

The errors in the wavefunctions, the position density, and the spin density are shown in Figure 4, from which we see clearly that the errors in the wavefunctions increase as $\varepsilon \to 0$, while the errors in the position density and the spin density stay almost unchanged. We then repeat the test for the coupling strength $\eta = 1$, and we observe the same tendency. Therefore, we have numerically verified that the TSSP method with unresolved time steps can give correct physical observables. It is worth emphasizing that the analysis for this property is open when $\eta = 1$, so the tests here can only serve as numerical evidence.

Example 4.2. In this example, we demonstrate the accuracy of the TSSP method applied to the Pauli equation in two dimensions. We choose the following WKB-type initial condition:

$$\begin{aligned}\psi_+(x_1,x_2,0) &= \psi_-(x_1,x_2,0)\\ &= \exp\left(i\frac{x_1-1}{\varepsilon}\right)\exp\left(i\frac{x_2-1}{\varepsilon}\right)\exp\left(-\frac{(x_1-1)^2+(x_2-1)^2}{2\varepsilon}\right).\end{aligned}$$

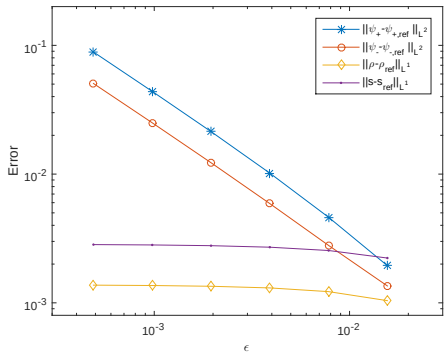

(a) $\eta = \varepsilon$

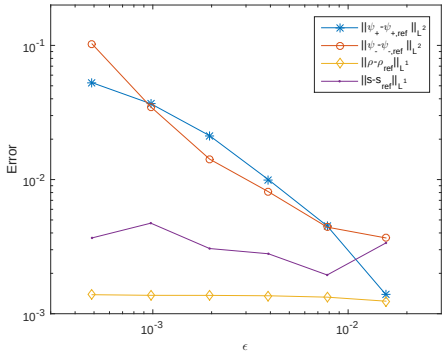

(b) $\eta = 1$

FIG. 4. *Capturing observables with ε-independent Δt.* (a): $\eta = \varepsilon$, $\varepsilon = \frac{1}{64}, \frac{1}{128}, \frac{1}{256}, \frac{1}{512}, \frac{1}{1024}$, *and* $\frac{1}{2048}$, $\Delta t = \frac{1}{25}$, $\Delta x = \frac{2\pi\varepsilon}{64}$. (b): $\eta = 1$, $\varepsilon = \frac{1}{64}, \frac{1}{128}, \frac{1}{256}, \frac{1}{512}, \frac{1}{1024}$, *and* $\frac{1}{2048}$, $\Delta t = \frac{1}{25}$, $\Delta x = \frac{2\pi\varepsilon}{64}$.

Roughly speaking, this initial condition denotes a semiclassical spinor localized around $\boldsymbol{x} = (1, 1)$ moving with speed $(1, 1)$. We choose the computation domain to be $[0, \pi] \times [0, \pi]$ so that periodic conditions can be imposed with negligible error. We also choose the following potentials and magnetic field:

$$V = 0, \quad \mathbf{A} = (0, 0), \quad \mathbf{B} = (\sin(x), \cos(y), 1).$$

Since we treat this example as a test model for the Pauli equation in two dimensions, no relation between $\mathbf{A}$ and $\mathbf{B}$ is assumed. In particular, we have chosen trivial V and $\mathbf{A}$ to underline the effect of the Stern–Gerlach term. Unless specified, the coupling strength η is set to be 1.

We first fix $\varepsilon = \frac{1}{32}$, and then compute the numerical solutions with resolved mesh $\Delta x = \frac{\pi\varepsilon}{32}$, $\Delta t = \frac{0.4\varepsilon}{16}$. We plot some snapshots of (the real part of) the wavefunctions together with the flow map of (the first two components of) the spin density in Figure 5.

Next we fix $\varepsilon = \frac{1}{64}$, and then compute the numerical solutions up to $t = 0.5$ with two different mesh strategies, namely, the one with unresolved Δt,

$$\Delta x = \frac{\pi\varepsilon}{32}, \quad \Delta t = \frac{1}{20}$$

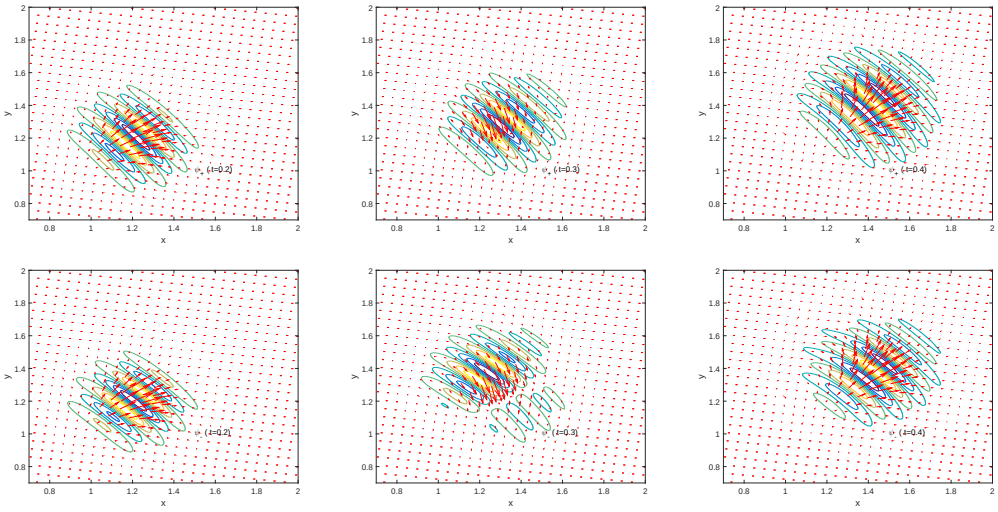

FIG. 5. *Snapshots of (the real part of) the wavefunctions together with the flow map of (the first two components of) the spin density.* $\varepsilon = \frac{1}{32}$, $\Delta x = \frac{\pi\varepsilon}{32}$, $\Delta t = \frac{0.4\varepsilon}{16}$. *Top Row:* ψ_+ *for* $t = 0.2$, 0.3, *and* 0.4. *Bottom Row:* ψ_- *for* $t = 0.2$, 0.3, *and* 0.4.

and the one with resolved Δt,

$$\Delta x = \frac{\pi\varepsilon}{32}, \quad \Delta t = \frac{0.5\varepsilon}{16},$$

which gives the reference solutions. We plot the position density of each wavefunction with the flow map of (the first two components of) the spin density in Figure 6, from which we see obviously great agreement. Hence, we have again verified that ε-independent time steps can be used to calculate correct physical observables.

4.2. The Schrödinger–Landau–Lifshitz system. In this section, we test the TSSP method for the Schrödinger equation and the Gauss–Seidel projection method for the Landau–Lifshitz equation to understand spin and magnetization dynamics under different coupling regimes. For simplicity, we only consider one-dimensional space. Since the exact solution is not available in this case, we have ascertained that the results below are unchanged by refining both the spatial meshes and the time steps.

Example 4.3 (Weak coupling). Set $\Omega = [0, 1]$. The external potential $V(x)$ is set to be $\frac{\sqrt{\varepsilon}}{x(x-1)}$ so that the electron is confined in Ω. The final time $t = 20$. $\Delta t = 1/512$, $\varepsilon = 1/256$, $h = 1/512$, $\Delta x = h/8$, and $\alpha = 0.1$. The coupling constant $\eta = 0.01$, which means the spin-magnetization coupling is weak. Initial conditions for the wavefunctions and magnetization are

$$\psi_+ = \psi_- = \frac{5}{\sqrt{\pi}} \exp\left(i\frac{0.1x}{\varepsilon}\right) \exp\left(-50(x-0.5)^2\right)$$

and

$$\boldsymbol{m}_0(x) = (\cos(x), \sin(x), 0),$$

respectively.

After the initial relaxation, the magnetization achieves its stable configuration, which is (almost) a constant field with the third component almost 0 (Figure 7(a)).

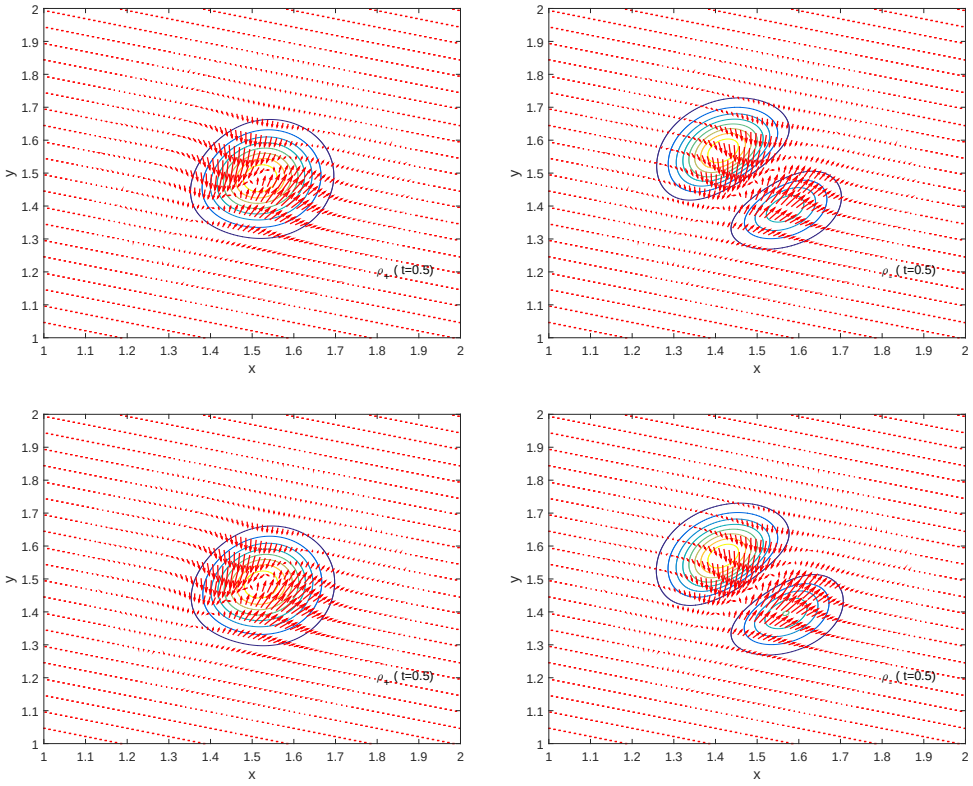

FIG. 6. *Comparison of the positition density of each wavefunction with the flow map of (the first two components of) the spin density. Top row: Solutions with unresolved* Δt. *Bottom row: Solutions with resolved* Δt.

The real parts of the spin-up and spin-down wavefunctions at $t = 20$ are plotted in Figure 7(b). We also observe that the spin swings in a certain direction after the initial relaxation. To get this direction, we calculate the angle between the spin where its maximum magnitude is achieved and the magnetization is at the same position; see Figure 8(a). At $t = 20$, we plot the magnetization and spin directions in Figure 8(b) and their projections along the x axis in Figure 8(c). The angle swings around 28°. Since the magnetization achieves its stable state at later times, the spin swings around 28° with respect to the magnetization.

In this case, $\eta = 0.01$ is small and the magnetization has a stable configuration, which is not affected by spin dynamics. This is consistent with the rigorous result of the semiclassical limit of (1) and (2) in the weak coupling regime [5].

Set the final time $t = 10000$. The long-time dynamics is shown in Figure 9. Again an (almost) periodic swing is observed for spin dynamics. The angle between spin and magnetization, where the maximum magnitude of spin is achieved, is around 0°. However, the spin shows a complicated configuration and is not just simply aligned with the magnetization.

Example 4.4 (Strong coupling). Set $\Omega = [0, 1]$. The external potential $V(x)$ is set to be $\frac{\sqrt{\varepsilon}}{x(x-1)}$ so that the electron is confined in Ω. The final time $t = 20$. $\Delta t = 1/512$,

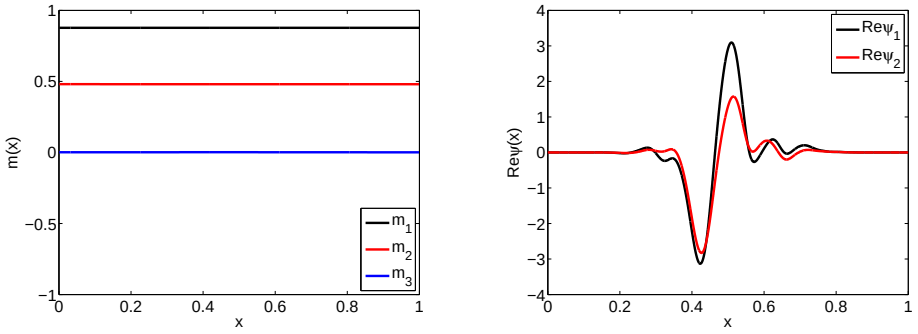

(a) Magnetization (b) Wavefunction

FIG. 7. *Configurations of magnetization and the real part of the wavefunctions at $t = 20$ when $\eta = 0.01$.* (a): *Magnetization.* (b): *Wavefunction.*

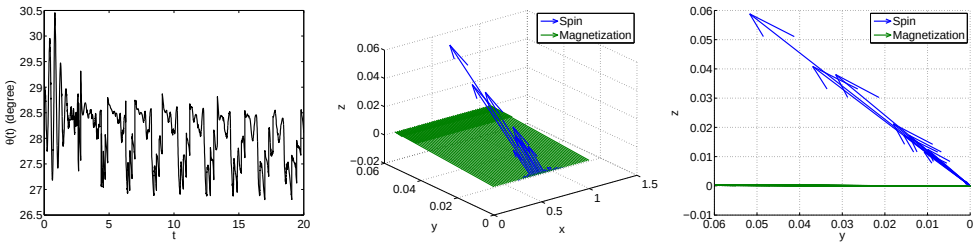

(a) Angle (b) Direction (c) Projection

FIG. 8. *Spin-magnetization angle in terms of time, arrow plot of spin and magnetization in three dimensions, and their projections along the x axis at $t = 20$. An (almost) periodic swing is observed for spin dynamics when $\eta = 0.01$.* (a): *Angle.* (b): *Direction.* (c): *Projection.*

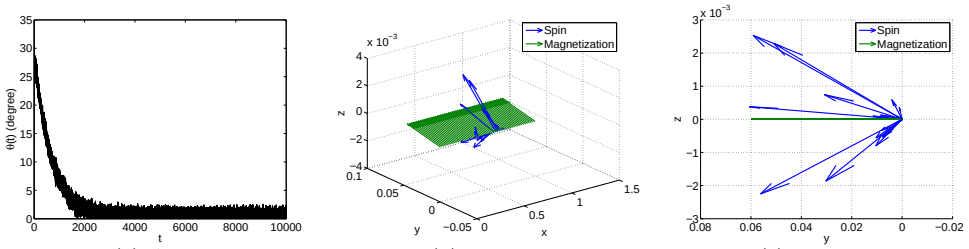

(a) Angle (b) Direction (c) Projection

FIG. 9. *Spin-magnetization angle in terms of time, arrow plot of spin and magnetization in three dimensions, and their projections along the x axis at $t = 10000$. An (almost) periodic swing with the angle $0°$ is observed for spin dynamics when $\eta = 0.01$ if time is long enough. The spin is not just simply aligned with the magnetization.* (a): *Angle.* (b): *Direction.* (c): *Projection.*

$\varepsilon = 1/256$, $h = 1/512$, $\Delta x = h/8$, and $\alpha = 0.1$. The coupling constant $\eta = 10$, which means the spin-magnetization coupling is strong. Initial conditions for the wavefunctions and magnetization are

$$\psi_+ = \psi_- = \frac{5}{\sqrt{\pi}} \exp\left(i\frac{0.1x}{\varepsilon}\right) \exp\left(-50(x-0.5)^2\right)$$

and

$$\boldsymbol{m}_0(x) = (\cos(x), \sin(x), 0),$$

respectively.

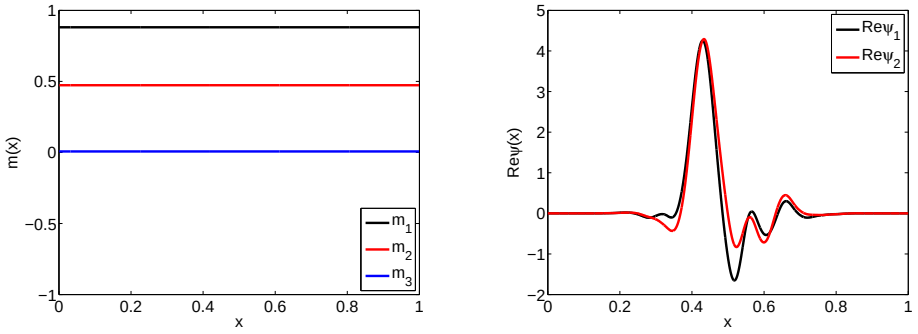

(a) Magnetization (b) Wavefunction

FIG. 10. *Configurations of magnetization and the real part of wavefunctions at* $t = 20$ *when* $\eta = 10$. (a): *Magnetization;* (b): *Wavefunction.*

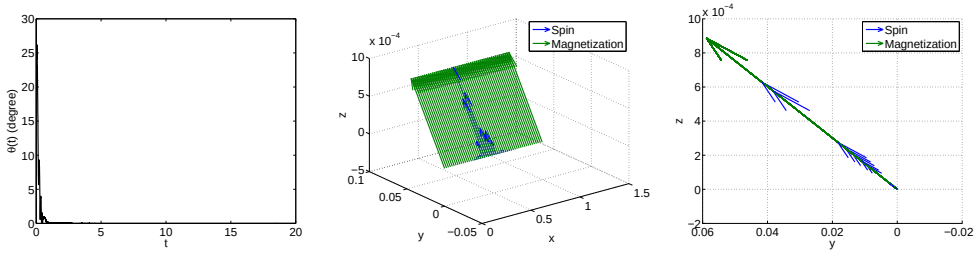

(a) Angle (b) Direction (c) Projection

FIG. 11. *Spin-magnetization angle in terms of time, arrow plot of spin and magnetization in three dimensions, and their projections along the* x *axis at* $t = 20$. *An (almost) periodic swing is observed for spin dynamics when* $\eta = 10$. (a): *Angle.* (b): *Direction.* (c): *Projection.*

After the initial relaxation, the magnetization achieves its stable configuration, which is (almost) a constant field (Figure 10(a)). The real parts of the spin-up and spin-down wavefunctions at $t = 20$ are plotted in Figure 10(b). We calculate the angle between the spin where its maximum magnitude is achieved and the magnetization is at the same position; see Figure 11(c). The angle drops to 0 quickly and a perfect alignment between spin and magnetization is observed. This is consistent with the physical intuition [17].

5. Conclusion and perspectives. In this paper, we have made two major contributions. We have established a dynamical model for the spin density and the magnetization coupling phenomenon from a variational perspective and constructed a hybrid numerical method for the Schrödinger–Landau–Lifshitz system, where the time splitting spectral method for the quantum wavefunction has been rigorously analyzed. In accordance with our simulations, in the weak coupling regime, $\eta = O(\varepsilon)$, the magnetization configuration first evolves to a stable configuration, and the interaction between the spin density and the magnetization is not manifestly noticeable until $t = O(\frac{1}{\varepsilon})$. However, in the strong coupling regime, $\eta = O(1)$, the magnetization and the spin density reach their respective stable configurations within $O(1)$ time, where the angle between the principal direction of the spin density and that of the magnetization is approaching zero, which demonstrates the alignment phenomenon.

In the future, we may explore the existence and asymptotic behavior of the solutions to the Schrödinger–Landau–Lifshitz system and design better numerical methods for the Landau–Lifshitz equation.

Acknowledgments. J. Chen, J. Liu, and Z. Zhou would like to thank Harold U. Baranger and Lihui Chai for helpful discussions.

REFERENCES

[1] M. N. Baibich, J. M. Broto, A. Fert, F. N. Van Dau, F. Petroff, P. Etienne, G. Creuzet, A. Friederich, and J. Chazelas, *Giant magnetoresistance of* $(001)Fe/(001)Cr$ *magnetic superlattices*, Phys. Rev. Lett., 61 (1988), pp. 2472–2475, doi:10.1103/PhysRevLett.61.2472.

[2] W. Bao, S. Jin, and P. A. Markowich, *Spectral approximations for the Schrödinger equation in the semi-classical regime*, J. Comput. Phys., 175 (2002), pp. 487–524, doi:10.1006/jcph.2001.6956.

[3] A. Brataas, A. D. Kent, and H. Ohno, *Current-induced torques in magnetic materials*, Nat. Mater., 11 (2012), pp. 372–381, doi:10.1038/nmat3311.

[4] W. F. Brown Jr., *Micromagnetics*, Wiley, New York, 1963.

[5] L. Chai, C. J. García-Cervera, and X. Yang, *Semiclassical Limit of the Schrödinger-Poisson-Landau-Lifshitz-Gilbert System*, preprint, 2016.

[6] J. Chen, C. J. García-Cervera, and X. Yang, *Mean-field dynamics of the spin-magnetization coupling in ferromagnetic materials: Application to current-driven domain wall motions*, IEEE Trans. Magn., 51 (2015), pp. 1–6, doi:10.1109/TMAG.2015.2401534.

[7] J. Chen, C. J. García-Cervera, and X. Yang, *A mean-field model of spin dynamics in multilayered ferromagnetic media*, Multiscale Model. Simul., 13 (2015), pp. 551–570, doi:10.1137/140953149.

[8] R. Cheng and Q. Niu, *Microscopic derivation of spin-transfer torque in ferromagnets*, Phys. Rev. B, 88 (2013), 024422, doi:10.1103/PhysRevB.88.024422.

[9] T. L. Gilbert, Phys. Rev., 100 (1955), p. 1243. [Abstract only; full report, Armor Research Foundation Project No. A059, Supplementary Report, May 1, 1956 (unpublished)].

[10] L. Greengard and J. Y. Lee, *Accelerating the nonuniform fast Fourier transform*, SIAM Rev., 46 (2006), pp. 443–454, doi:10.1137/S003614450343200X.

[11] P. Grünberg, R. Schreiber, Y. Pang, M. B. Brodsky, and H. Sowers, *Layered magnetic structures: Evidence for antiferromagnetic coupling of Fe layers across Cr interlayers*, Phys. Rev. Lett., 57 (1986), pp. 2442–2445, doi:10.1103/PhysRevLett.57.2442.

[12] B. Guo and S. Ding, *Landau–Lifshitz Equations*, World Scientific, Singapore, 2008.

[13] A. Hubert and R. Schäfer, *Magnetic Domains: The Analysis of Magnetic Microstructures*, Springer, Berlin, 1998.

[14] I. Žutić, J. Fabian, and S. Das Sarma, *Spintronics: Fundamentals and applications*, Rev. Mod. Phys., 76 (2004), pp. 323–410, doi:10.1103/RevModPhys.76.323.

[15] S. Jin, P. A. Markowich, and C. Sparber, *Mathematical and computational methods for semiclassical Schrödinger equations*, Acta Numer., 20 (2011), pp. 121–209, doi:10.1017/S0962492911000031.

[16] S. Jin and Z. Zhou, *A semi-Lagrangian time splitting method for the Schrödinger equation with vector potentials*, Commun. Inf. Syst., 13 (2013), pp. 247–289, doi:10.4310/CIS.2013.v13.n3.a1.

[17] J. I. Kaplan, *Diffusion constant in the effective Bloch equation for ferromagnetic resonance in metals*, Phys. Rev., 143 (1966), pp. 351–352, doi:10.1103/PhysRev.143.351.

[18] L. Landau and E. Lifshitz, *On the theory of the dispersion of magnetic permeability in ferromagnetic bodies*, Physikalische Zeitschrift der Sowjetunion, 8 (1935), pp. 153–169.

[19] Z. Ma, Y. Zhang, and Z. Zhou, *An improved semi-Lagrangian time splitting spectral method for the semi–classical Schrödinger equation with vector potentials using NUFFT*, Appl. Numer. Math., 111 (2017), pp. 144–159.

[20] G. Panati, H. Spohn, and S. Teufel, *Effective dynamics for Bloch electrons: Peierls substitution and beyond*, Commun. Math. Phys., 242 (2003), pp. 547–578, doi:10.1007/s00220-003-0950-1.

[21] G. Panati, H. Spohn, and S. Teufel, *Motions of electrons in adiabatically perturbed periodic structures,* Analysis, Modeling and Simulation of Multiscale Problems, Springer, Berlin, 2006, pp. 595–617.

[22] Y. Qi and S. Zhang, *Spin diffusion at finite electric and magnetic fields*, Phys. Rev. B, 67 (2003), 052407, doi:10.1103/PhysRevB.67.052407.

[23] D. C. Ralph and M. D. Stiles, *Spin transfer torques*, J. Magn. Magn. Mater., 320 (2008), pp. 1190–1216, doi:10.1016/j.jmmm.2007.12.019.

[24] X.-P. Wang, C. J. García-Cervera, and W. E, *A Gauss–Seidel projection method for micromagnetics stimulations*, J. Comput. Phys., 171 (2001), pp. 357–372, doi:10.1006/jcph.2001.6793.

[25] S. Zhang, P. M. Levy, and A. Fert, *Mechanisms of spin-polarized current-driven magnetization switching*, Phys. Rev. Lett., 88 (2002), 236601, doi:10.1103/PhysRevLett.88.236601.

[26] S. Zhang and Z. Li, *Roles of nonequilibrium conduction electrons on the magnetization dynamics of ferromagnets*, Phys. Rev. Lett., 93 (2004), 127204, doi:10.1103/PhysRevLett.93.127204.